AD_____

Award Number: W81XWH-10-1-0112

TITLE: Epithelial and Stromal Spectral Imaging for Rapid Surgical Margin Analysis

PRINCIPAL INVESTIGATOR: Ashley Laughney

CONTRACTING ORGANIZATION: Dartmouth College
Hanover, NH 03755-1404

REPORT DATE: March 2013

TYPE OF REPORT: Annual Summary

PREPARED FOR: U.S. Army Medical Research and Materiel Command
Fort Detrick, Maryland 21702-5012

# REPORT DOCUMENTATION PAGE

*Form Approved*
*OMB No. 0704-0188*



| **1. REPORT DATE** | **2. REPORT TYPE** | **3. DATES COVERED** |
|---|---|---|
| March 2013 | Annual Summary | 1 March 2010 – 28 February 2013 |

**4. TITLE AND SUBTITLE**

Epithelial and Stromal Spectral Imaging for Rapid Surgical Margin Analysis

**5a. CONTRACT NUMBER**

**5b. GRANT NUMBER**
W81XWH-10-1-0112

**5c. PROGRAM ELEMENT NUMBER**

**6. AUTHOR(S)**

Ashley Laughney

**E-Mail:** Laughney.Ashley@mgh.harvard.edu

**5d. PROJECT NUMBER**

**5e. TASK NUMBER**

**5f. WORK UNIT NUMBER**

**7. PERFORMING ORGANIZATION NAME(S) AND ADDRESS(ES)**

Dartmouth College
Hanover, NH 03755-1404

**8. PERFORMING ORGANIZATION REPORT NUMBER**

**9. SPONSORING / MONITORING AGENCY NAME(S) AND ADDRESS(ES)**
U.S. Army Medical Research and Materiel Command
Fort Detrick, Maryland 21702-5012

**10. SPONSOR/MONITOR'S ACRONYM(S)**

**11. SPONSOR/MONITOR'S REPORT NUMBER(S)**

**12. DISTRIBUTION / AVAILABILITY STATEMENT**
Approved for Public Release; Distribution Unlimited

**13. SUPPLEMENTARY NOTES**

**14. ABSTRACT**

A new, scanning beam spectroscopy platform was developed to dramatically improved image acquisition speed of localized light scattering. The new scanning in situ spectroscopy platform samples broadband reflectance from a 150μm diameter spot over a 1cm2 field using a dark field geometry and telecentric lens; the system was designed to balance sensitivity to stromal and epithelial distributions, while sufficiently imaging the inherent diversity within a diagnosis. The diagnostic performance of this new imaging system was tested in 29 tissues procured during breast conservative surgery. Nearly 300,000 broadband spectra were parameterized using light scattering models and spatially dependent spectra signatures were interpreted using co-occurrence matrix representation of image texture. Local scattering changes distinguished benign from malignant pathologies with 94% accuracy, 85% sensitivity, 100% specificity, and 100% positive & 90% negative predictive value, using a threshold-based classifier. Texture and shape features offered unique information about scattering ultra-structures, and suggest a potential contrast mechanism for ductal carcinoma in situ. Images of localized scattering readily identify benign and malignant pathologies in resected specimens and offer new spectral-spatial signatures of clinically relevant breast pathologies.

**15. SUBJECT TERMS**

| **16. SECURITY CLASSIFICATION OF:** | | | **17. LIMITATION OF ABSTRACT** | **18. NUMBER OF PAGES** | **19a. NAME OF RESPONSIBLE PERSON** |
|---|---|---|---|---|---|
| **a. REPORT** | **b. ABSTRACT** | **c. THIS PAGE** | | | USAMRMC |
| U | U | U | UU | 15 | **19b. TELEPHONE NUMBER** *(include area code)* |

## Table of Contents

**Page**

## Introduction

Local management of breast cancer has been hindered by an inability to intra-operatively assess tumor margin status, predominantly because use of frozen sections are limited by freezing artifacts in adipose tissues (1, 2) and reported sensitivities for touch-preparation cytology have been inconsistent (3). A scanning in situ spectroscopy platform was designed to evaluate nearly coherent scatter-imaging signatures of breast tissue pathologies. Its spot size was constrained by light transport principles to ~100μm and the scanning-beam approach to spectral image acquisition yielded rapid, full coverage of pathologically relevant field sizes ($1cm^2$). As previously reported, spectroscopic image features from $1mm^2$ areas were diagnostically discriminant and enabled quantification of known tissue heterogeneities. However, the field of view (FOV) can be too small to evaluate surgical tissues in a reasonable timeframe, as resected tissues may contain tumors up to 5cm in diameter surrounded by a targeted layer of grossly normal tissue that is nearly 1cm thick. Ideally, the full tumor specimen could be assessed in a non-contact manner, while maintaining sensitivity to the tumor-specific features in localized volumes. As an extension of this concept, a specialized near-infrared (NIR) planar imaging modality, pioneered by the University of California at Irvine (UCI) and commercialized by Modulated Imaging Inc., was investigated to sample localized scattering signatures over a wide field in the spatial frequency domain. Spatial frequency domain imaging (SFDI) resolved sub-surface tissue optical properties using a harmonically varying plane wave source and analysis of the spatial-modulation transfer function (s-MTF)(4). Structured illumination patterns enhanced signal localization and the spatial frequency dependence of diffuse reflectance was used to uniquely separate absorption and scattering effects. High spatial frequencies were sensitive to short pathlength phenomenon, primarily scattering by local fluctuations in tissue morphology. Continuous illumination was sensitive to both absorption and scattering. The spatial frequency of the illumination pattern integrated optical property determination with volume averaging in depth and preserved signal localization in this diffuse acquisition geometry. Here, higher spatial frequencies were probed (up to 0.33mm-1) for improved sensitivity to local scattering by tissue ultra-structure and for resolving depths appropriate for margin assessment. SFDI detects photons that are neither coherent nor diffuse, and probes optical parameters complimentary to those sampled by the scanning in situ spectroscopy platform. Here, we show its more volume-averaged measures can also distinguish tissue-types and correlate with tissue epithelial and stromal distributions, measured quantitatively by immunohistochemistry.

## Body

*Task 1. Assemble and parameterize an extensive databank of scatter spectra from fresh breast tissue across clinically relevant diagnostic categories.*

The ability of SFDI to distinguish histopathology, here used as the diagnostic gold standard, was evaluated at the surface of 47 surgical breast tissues. In this HIPAA-compliant, prospective study, approved by Institutional Review Board for the protection of human subjects, written informed consent was not required for participants, although an information sheet regarding the study was provided with an opt-out provision. Fresh tissue procured during breast conserving surgery was obtained directly from the Department of Pathology at DHMC from patients who did not decline this use of their tissues. Specimen imaging did not affect procedure time in the operating room or the content and verification of the final pathology report. Tissues were imaged within 30 minutes of resection and returned to pathology for standard histological processing. In the case of larger lumpectomy specimens, the three-dimensional tissue volume was cut in a 'bread loaf' pattern (standard pathology protocol) and one face of one slice of the tissue was imaged. Figure 1 illustrates co-registration between photographs of the intact, surgical breast tissue (row 1), subsequent histopathology (row 2), and spectral images (rows 3-7). An experienced breast pathologist (WAW) outlined a microscopic diagnosis on digital photographs of each specimen, guided by co-registered Hematoxylin and Eosin (H&E) stained tissue sections from the imaged surface. Affine transformations were manually performed in Photoshop to directly transform these regions into masks for region-based analysis in MATLAB. A total of 48 specimens from 47 patients were consecutively imaged in this study; one was excluded from analysis because surgical inks bled into the primary tissue field. Surgical inks, sometimes observed at the tissue edge, were avoided during ROI selection and masked according to the R2–coefficient of determination (pixels excluded if $R2<0.95$). Over 265,000 spatial frequency- and wavelength-dependent reflectance measures were evaluated in 59 regions of interest (ROI). Discrimination was assessed between benign and malignant pathologies and between the benign pathology subtypes, normal/fibrocystic disease and fibroadenoma, and the malignant pathology subtypes, DCIS, invasive cancer, and treated invasive cancer (residual disease following chemotherapy), as listed in Table 1. Tumors treated with neoadjuvant chemotherapy prior to surgical resection (n=5) were also imaged to observe how chemotherapy alters tissue optical properties to better inform diffuse tomographic monitoring of treatment response to therapy (5). Spectroscopic scattering and absorption parameter images, co-registered with a digital photograph of the breast tissue, are shown in Figure 1 for all represented tissue types.

| Diagnosis | # ROI | # Reflectance Measures | |
|---|---|---|---|
| *Normal/Fibrocystic (NOR)** | 22 | 109,841 | ***Benign*** **170,158** |
| *Fibroadenoma (FA)** | 11 | 60,317 | |
| *Ductal carcinoma in situ (DCIS)* | 4 | 8,487 | ***Malignant*** **94,916** |
| *Invasive cancer (INV)* | 17 | 63,552 | |
| *Invasive cancer, treated (INV,Rx)* | 5 | 22,877 | |
| **Totals** | **59** | | **265,074** |

**Table 1 Total numbers of ROI and modulated reflectance spectra assessed per diagnostic class. Benign pathologies analyzed include normal or fibrocystic tissues and fibroadenomas (*). Malignant pathologies analyzed include DCIS, invasive cancer and treated invasive cancers.**

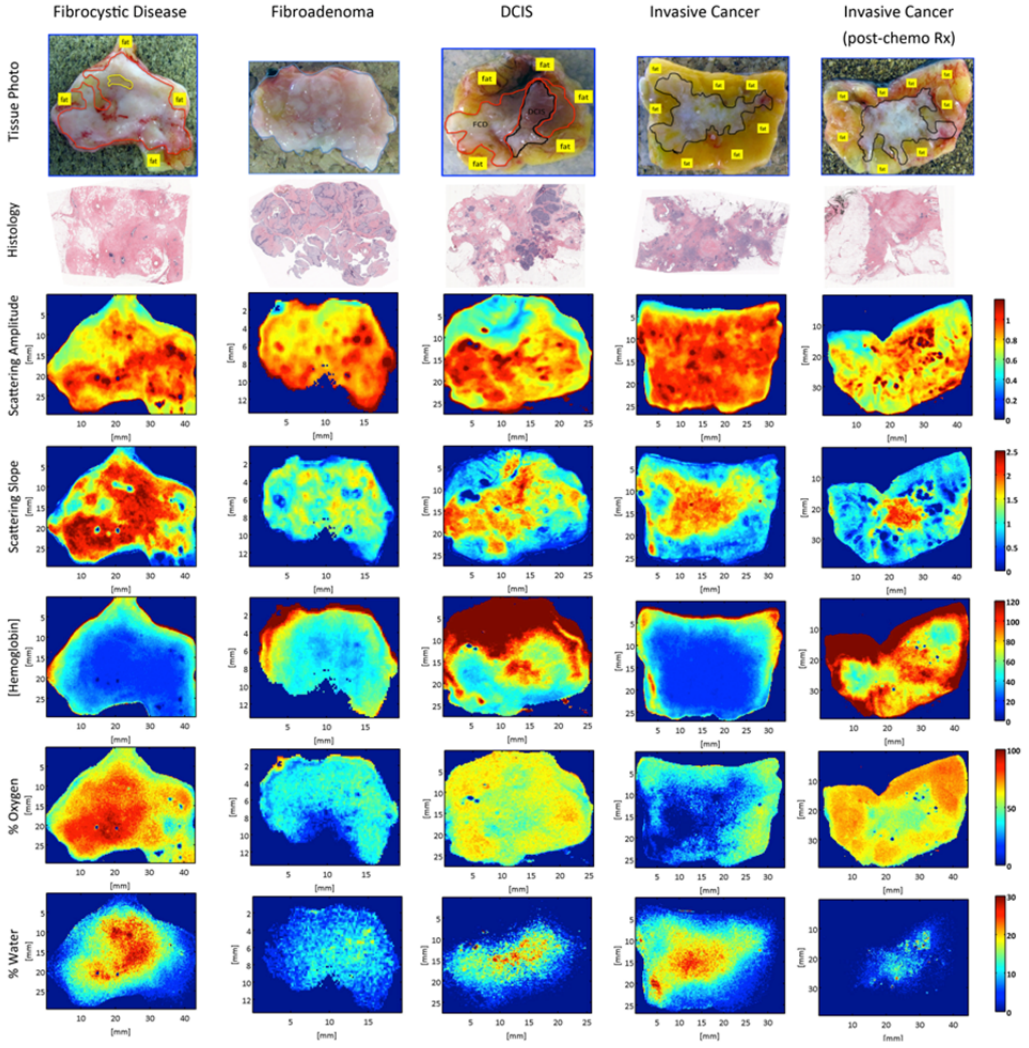


**Figure 1 Spectral parameter maps corresponding to the pathology subtypes: fibrocystic disease, fibroadenoma, DCIS, invasive cancer and treated invasive cancer. Row 1 is a tissue photograph, row 2 is the corresponding histology, row 3 is the scattering amplitude maps, row 4 is the scattering slope maps, row 5 is the hemoglobin concentration maps, row 6 is the percent oxygen maps and row 7 is the percent water maps.**

Spectral parameters were associated with morphological and immunohistochemical markers identified in adjacent, stained sections of the tissue, cut in the exact geometry imaged in situ. All tissue was fixed in 10% buffered formalin (Biochemical Science Inc, Swedesboro, NJ), dehydrated through graded alcohols, and paraffin embedded. Tissue sections (4μm) were coated with adhesive (Sta-onTM, Surgipath Medical Industries, Inc, Richmond IL), mounted on glass slides, and stained with Hematoxylin and Eosin (H&E) for initial review. Tissue sections were air dried for at least 30 minutes and then loaded onto a Leica Bond Max automated immunostainer. Here the sections were baked (30 minutes at 60ºC), de-waxed for 30 minutes at 72°C, rinsed with alcohol and washed in Bond wash buffer. Antigen retrieval used Bond epitope Retrieval 2 Cat # Ar9640 (pH 8.9-9.1) for 20 minutes at 100°C; followed by cooling for 12 minutes and a rinse in Bond wash buffer. All de-waxed, antigen retrieval and detection reagents were supplied by Leica Microsystems (Bannockburn, IL). The primary antibodies were incubated for 15 minutes - CK5D3 at 1:100 (Biogenix, Fremont CA), CD31 at 1:50 (Dako, Carpinteria, CA), and CD105 at 1:60 (Vector, Burlingame, CA). Diaminobenzidine was applied for visualization with a Hematoxylin counterstain. Mean vessel density (MVD) was quantified according to the areas of CD31-positive or CD105-positive vessels, segmented in pseudo-color, as a percentage of the total slide area. Mean vessel area (MVA) was quantified according to the combined areas of CD31-positive or CD105-positive blood vessels, segmented in pseudo-color and measured in μm2. CD31 (platelet endothelial cell adhesion molecule) was used to stain pre-existing endothelial cells as an indicator of normal vasculature, even though malignant vessels can also retain this antigen (6). CD105 (Endoglin) was used to stain a trans-membrane glycoprotein expressed predominantly on the surface of highly proliferating endothelial cells as an indicator of tumor angiogenesis; it is thought to antagonize the inhibitory effects of TGF-ß on cell proliferation and capillary formation (6). Whole H&E and immunostained slides were digitally scanned at high resolution and montaged together using the Surveyor© Automated Specimen Scanning stage control bundled software (Objective Imaging Ltd., Cambridge UK). Possible correlates between immunohistochemical measures and spectral parameters were evaluated according to the Pearson's correlation coefficient. Spectral parameters and quantitative immunohistochemistry distributions are summarized in Figure 2. Pairwise correlations between spectral parameters and quantitative immunohistochemistry are summarized in Table 2.

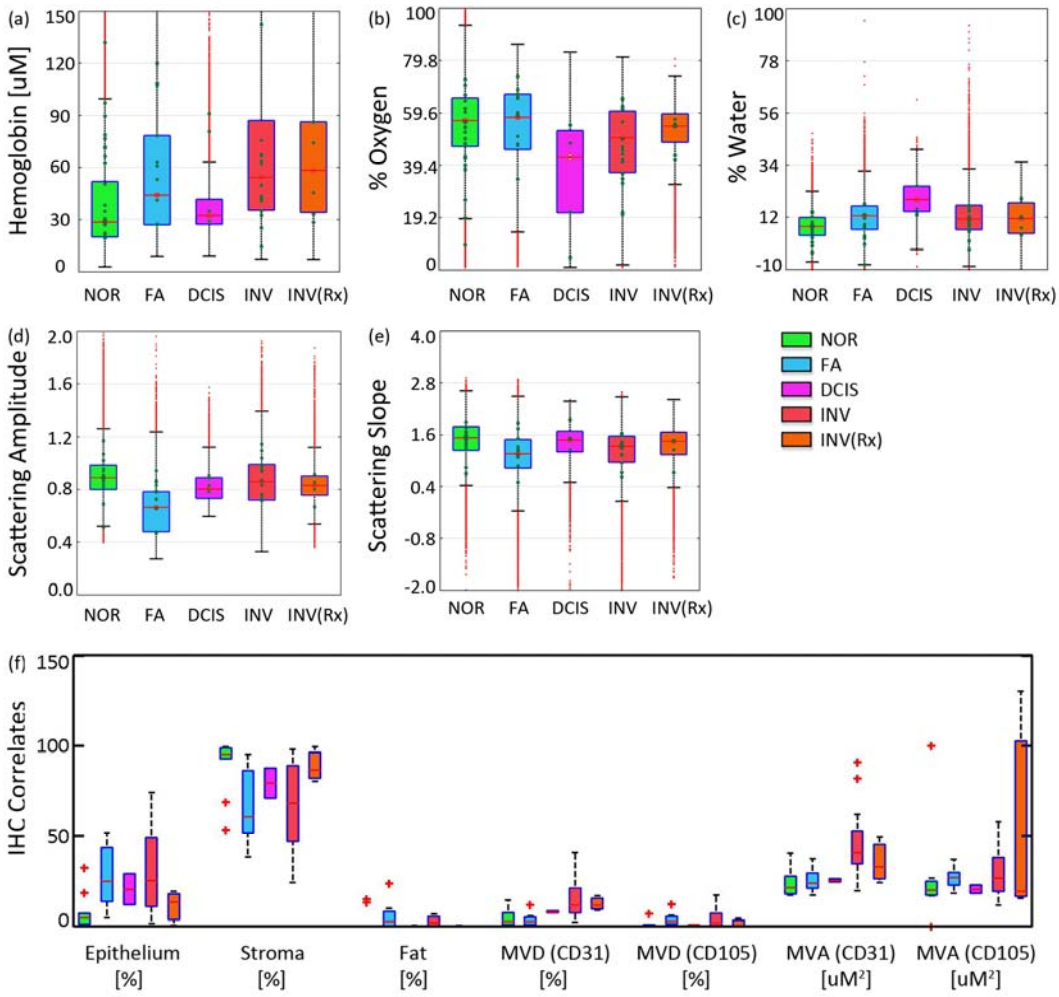


**Figure 2 (a-e) Recovered spectral parameters for all tissues per pathology subtype, indicated by color: *fibrocystic disease* (green), *fibroadenoma* (blue), *DCIS* (pink), *invasive cancer* (red) and *treated invasive cancer* (orange). (f) Corresponding immunohistochemical measures of percent stroma, epithelium and fat, and CD31-positive, CD105-positive vascular density and area.**

| | A | b | [HbT] | % $O_2$ | % $H_2O$ |
|---|---|---|---|---|---|
| **% Epithelium** | -0.06 | **-0.37** | **0.27** | -0.11 | -0.21 |
| **% Stroma** | 0.06 | **0.33** | **-0.28** | 0.09 | **0.25** |
| **% Fat** | -0.02 | -0.01 | 0.21 | 0.02 | **-0.28** |
| **Total Mean Vessel Density** | 0.18 | **-0.42** | **0.37** | -0.19 | 0.00 |
| **Total Mean Vessel Area** | 0.01 | **-0.34** | 0.12 | **-0.28** | 0.02 |

**Table 2 Spectral-immunohistochemical correlates**
**The Pearson's correlation coefficient tabulated for spectral-immunohistochemical pairs. Negative and positive correlations greater than 20% are highlighted in red and green respectively.**

Collagen in the extracellular stroma demonstrated a strong, positive correlation with scattering slope because the small fibrils that form collagen fibers further enhance Rayleigh-type scattering (7). In contrast, a strong negative correlation was observed between tissue epithelial content and the scattering slope. Malignant tissues expressed greater levels of angiogenic vessels and pre-existing vascular endothelium. This net growth in vascularity was detected spectroscopically by increased total hemoglobin, but no optical distinction was made between CD105-specific and CD31-specific vasculature. Immunohistochemical measures were sampled in discrete locations about the tissue surface, limiting its complete representation of ROIs.

*Task 2. Develop an automated classification algorithm to provide real-time, un-biased interpretation of scatter images for improved evaluation of breast surgical margins*.

Over 265,000 SFDI spectral parameter sets were applied to the previously developed, discriminant classifier (nearest-neighbor learning algorithm) and separation of all tissue subtypes was achieved with 82% accuracy. Automated spectral discrimination was assessed between benign and malignant pathologies and all pathology subtypes listed in Table 1; performance was evaluated using a threefold cross-validation (8). The nearest-neighbor algorithm assigned each unclassified parameter set to the majority diagnosis of its k nearest neighbors found in the training space by an efficient k-dimensional tree search algorithm (9). A whitening transformation was applied to all spectral parameters prior to diagnostic discrimination to prevent amplitude weighting. Additionally, outliers were removed from the training set according to their inter-quartile fractions. Query points were never marked as outliers because this information was not known a priori. Receiver operating characteristic (ROC) analysis was used to optimize classifier sensitivity and bias as a function of nearest neighbor number, k. Classification error was taken to be the percentage of misclassified pixels in the validation set, where a misclassification means that the diagnosis assigned by the classifier did not match the diagnosis provided by the pathologist. Reported diagnostic performance values were averaged over the three executions. Confidence intervals ($\alpha$=0.05) for the sensitivity and specificity were computed according to the Yates $\chi$2 interval (10). Diagnostic performance is summarized in Table 3, which reports the sensitivity, specificity, positive predictive value (PPV), negative predictive value (NPV) and accuracy observed per tissue type. Discrimination of benign from malignant pathologies was highly specific (93%) and reasonably sensitive (79%), although sensitivity was limited in under-represented pathologies like DCIS and treated invasive cancers (61-66%). Discrimination between benign and malignant pathologies was more accurate (88%) because these classes were better represented in training.

| | NOR | FA | DCIS | INV | INV (Rx) | Benign vs. Malignant |
|---|---|---|---|---|---|---|
| **Sensitivity** | 0.90 | 0.87 | 0.61-0.65 | 0.71-0.73 | 0.64-0.66 | 0.79 |
| **Specificity** | 0.89 | 0.95 | 0.99 | 0.94 | 0.97 | 0.93 |
| **PPV** | 0.85 | 0.84 | 0.76 | 0.80 | 0.70 | 0.86 |
| **NPV** | 0.93 | 0.96 | 0.99 | 0.91 | 0.97 | 0.89 |
| ***Accuracy*** | 0.82 | | | | | 0.88 |

**Table 3 Summary of diagnostic performance per tissue type for discrimination between all tissue subtypes and for discrimination between benign and malignant pathologies; the 95% confidence interval is reported for sensitivity and specificity values when the confidence interval range exceeds 1%.**

An iterative search algorithm, Sequential Floating Forward Selection (SFFS), was implemented to rank the contribution of each spectral parameter to tissue type discrimination. The Bhattacharyya statistical distance, Jij, was used to measure the separation between two diagnostic classes (i,j) (11, 12) and this was generalized to all spectral parameters (n=5) by:

$$J = \sum_{i=1}^{5} \sum_{j=1}^{5} P_i P_j J_{ij}$$

Here, Pi represents the prior probability of class i determined by its fraction of pixels in the training set. The search algorithm ranked all parameters in order of the contribution to diagnostic class separability. The SFFS algorithm ranked the region-averaged: (1) scattering amplitude, (2) percent water, (3) total hemoglobin concentration, (4) the scattering slope and (5) percent oxygen, as most significant to tissue type discrimination in that order. Region-averaged measures improved diagnostic accuracy by accounting for pixel-to-pixel variations within spectral images. The scattering amplitude was most valuable to pathology discrimination, even through the scattering slope was observed to better localize suspicious fibro-glandular lesions. The scattering slope was likely under-valued by the limitations of pathology co-registration. Oxygen contributed least to a diagnosis, likely because of its sensitivity to post-surgery imaging time.

*Task 3. Enhance the diagnostic utility of our system by investigating the micro-optical properties of breast tissue.*

Previously we demonstrated that spectral-spatial signatures locally sampled by the scanning in situ spectroscopy platform (~150μm detection spot size) enhanced diagnostic sensitivity to DCIS. For the relatively diffuse SFDI spectral maps, it was not clear if discriminating texture features could be ascertained and if so, at what length scale (in terms of both a neighborhood size and displacement vector length). To test this contrast mechanism for SFDI, texture features were computed over many length scales and the SFFS feature-ranking algorithm was used to identify the top 5 spectroscopic and/or texture parameters that maximized diagnostic class separability according to the Bhattacharyya statistical distance. Texture features were not observed to be diagnostic at any of the length scales investigated; locally resolved, discriminating spatial patterns were masked by the larger, sub-millimeter volumes sampled in the spatial frequency domain.

This highlights that the 150μm illumination-detection spot size employed by the scanning in situ spectroscopy platform enhanced diagnostic sensitivity and revealed new spectral-spatial signatures of breast pathologies. Finally, the discrimination capabilities of both systems were compared: both systems discriminated all pathology subtypes with 82% accuracy, but the scanning system demonstrated heightened sensitivity to invasive cancers (84% vs. 72%) when spectroscopic textural features guided each local diagnosis. Spectroscopic scattering signatures detected by the scanning in situ spectroscopy platform and SFDI were distinct from one another because the former sampled nearly coherent scattering in a limited angular backscattering region and the latter sampled nearly diffuse scattering integrated over nearly all backscattering angles.

## Key Research Accomplishments

- Region-based evaluation of scanned, spectroscopic scattering per 150μm spot size over a 1mm2 area were diagnostically discriminant (benign from malignant pathologies could be distinguished with 90% sensitivity and 93% specificity) and encoded new spectral-spatial patterns of disease that were diagnostic and enhanced sensitive to DCIS.
- Sub-millimeter volumes sampled by spatial frequency domain imaging masked these signatures, but its spectroscopic absorption and scattering parameters were discriminating when interpreted together using a nearest-neighbor learning algorithm. Benign and malignant pathologies were distinguished with 88% accuracy and all pathology subtypes were identified with 82% accuracy.
- Raster-scanned scattering signatures were readily diagnostic and more sensitive to pathology subtypes like DCIS, but SFDI performed comparably when combined with supervised learning methods and evaluated larger tissue fields. Both systems remain to be tested intra-operatively, but this work validates further development of spectroscopic imaging systems, in combination with supervised learning methods, for interventional procedures like breast conserving surgery.
- This work validates its continued translation towards imaging tumor specimens immediately ex vivo and at the time of primary surgery to significantly reduce the secondary excision rate.

## Reportable Outcomes

### *Training accomplishments*

Awarded Ph.D. in Engineering Sciences from Thayer School of Engineering at Dartmouth (June 2012)
Research Fellow at Harvard Medical School/Massachusetts General Hospital, Center for Systems Biology (August 2012)

### *Peer-reviewed publications*

**Laughney AM,** Krishnaswamy V, Rizzo EJ, Schwab MC, Barth RJ, Cuccia DJ, Tromberg BJ, Paulsen KD, Pogue, BW, Wells WA, "Spectral discrimination of breast pathologies *in situ* using spatial frequency domain imaging," Breast Cancer Research and Treatment (submitted Aug 2012)

V. Krishnaswamy, **Laughney AM,** Paulsen KD, Pogue BW, "A Scanning In Situ Spectroscopy Platform for Imaging Morphological Contrast in Lumpectomy Specimens," Optics Express (submitted 2012)

**Laughney AM,** Krishnaswamy V, Rizzo E, Schwab M, Barth R, Pogue BW, Paulsen KD, Wells WA, "Scatter spectroscopic imaging distinguishes breast pathologies in tissues relevant to surgical margin assessment," Clinical Cancer Research (in review).

**Laughney AM,** Krishnaswamy V., Garcia-Allende PB,Conde OM, Wells WA, Paulsen KD, Pogue BW, "Automated classification of breast pathology using local measures of broadband reflectance," JOURNAL OF BIOMEDICAL OPTICS (2010).

V. Krishnaswamy, **A. M. Laughney**, K. Paulsen, and B. Pogue, "A Dark-Field In Situ Scanning Spectroscopy Platform for Broadband Imaging of Resected Tissue," Optics Letters (accepted).

### *Conference Publications*

**Laughney, A**., Krishnaswamy, V., Wells, W., Paulsen, K., Pogue, B., "Optical assessment of pathology in surgically resected breast cancers" Proceedings of SPIE BiOS Conference, Biomedical Applications of Light Scattering V, San Francisco CA, January 2011.

**Laughney, A.,** Krishnaswamy , V., Garcia-Allende, P.B., Wells , W.A., Conde, O.M., Paulsen, K.D., Pogue, B.W., "Imaging Breast Pathology in situ using Broadband Scatter Spectroscopy and a K-Nearest Neighbor Classifier," Proceedings of the OSA BIOMED Conference, Bio-optics in clinical application, Miami FL, April 2010.

### *Presentations*

"Localized spectroscopic imaging for the detection and discrimination of surgical breast tissue pathologies," Thesis Presentation, Thayer, Spring 2012

"A spatially-modulated scatter imaging system to detect tumor-associated stroma," *Breast Tumor Board Conference at Dartmouth-Hitchcock Medical Center, Spring 2011.*

"Optical characterization of pathologies in surgically resected breast cancers," Biomedical Lecture Series, Thayer, Spring 2011.

"System design for optical characterization of tissue pathologies in situ," *NSF ADVANCE Workshop at Rice University, Fall 2010.*

"Optimizing spectral contrast in breast lesions relative to normal tissue for surgical guidance," *Thayer, Spring 2010.*

"Automated Classification of Breast Pathology using Local Measures of Broadband Reflectance," *Optical Society of America 2010 BIOMED Conference (Miami, Fl), Spring 2010; Beckman Institute at the University of California Irvine, Winter 2009.*

### *Research Opportunities Received*

2011 Biophotonics International Graduate Summer School
NSF ADVANCE Workshop at Rice University
Pathobiology of Cancer Workshop by the American Association of Cancer Research
Neukom Institute Travel Grant

## Conclusions

Two localized spectroscopic imaging methods were investigated to detect and discriminate microscopic pathologies at the surface of excised breast tissues in order to improve resection completeness during breast conserving surgery. A scanning in situ spectroscopy platform was designed to explore nearly coherent scatter-imaging signatures of breast pathologies by raster-scanning a 100μm spot over a 1cm2 field of view. Localized spectroscopic texture and shape signatures from 1mm2 areas were diagnostically discriminant (benign from malignant pathologies could be distinguished with 90% sensitivity and 93% specificity) and enabled quantification of known tissue heterogeneities. The second, near-infrared imaging technique, spatial frequency domain imaging (SFDI), was used to image fully resected tissues with wide-field localization according to the spatial modulation transfer function. Structured illumination patterns preserved signal localization in this diffuse acquisition geometry and were used to quantify sub-surface tissue absorption and scattering at greater depths. Malignant and benign tissues could be distinguished with 79% sensitivity and 93% specificity, and higher order pathology subtypes were identified with 82% accuracy by both systems. Discrimination was highly specific and mainly limited by sensitivity to under-represented pathologies. Raster-scanned scattering signatures were readily diagnostic and more sensitive to pathology subtypes like DCIS, but SFDI performed comparably when combined with supervised learning methods and evaluated larger tissue fields. These purposeful applications of localized spectroscopic imaging could enable rapid, optical assessment of microscopic pathology in intact surgical tissues and the data analysis program was designed to support the future development of spectral imaging tools.

## References


1. J. Ferreiro, J. Gisvold and D. Bostwick, "Accuracy of frozen section diagnosis of mammographically detected breast biopsies; results of 1,490 consecutive cases," Am J Surg Path 19(1267-1271 (1995)

2. J. Tinnemans, T. Wobbes and R. Holland, "Mammographic and histopathologic correlation of non-palpable lesions of the breast and reliability of frozen section diagnosis," Surg Gynecol Obstet 165(523-529 (1987)

3. A. Saarela, T. Paloneva, T. Rissanen and H. Kiminiemi, "Determinants of positive histologic margins and residual tumor after lumpectomy for early breast cancer: a prospective study with special reference to touch preparation cytology," J Surg Onc 66(4), (1997)

4. D. J. Cuccia, F. Bevilacqua, A. J. Durkin, F. R. Ayers and B. J. Tromberg, "Quantitation and mapping of tissue optical properties using modulated imaging," JOURNAL OF BIOMEDICAL OPTICS 14(2), (2009)

5. S. Kukretia, A. Cerussi, B. Tromberg and E. Gratton, "Intrinsic near-infrared spectroscopic markers of breast tumors," Dis. Markers 25(6), 281-290 (2008)

6. M. G. Pakalniskis, W. A. Wells, M. C. Schwab, H. M. Froehlich, S. Jiang, Z. Li, T. D. Tosteson, S. P. Poplack, P. A. Kaufman, B. W. Pogue and K. D. Paulsen, "Tumor Angiogenesis Change Estimated by Using Diffuse Optical Spectroscopic Tomography: Demonstrated Correlation in Women Undergoing Neoadjuvant Chemotherapy for Invasive Breast Cancer?," RADIOLOGY 259(2), 365-374 (2011)

7. I. S. Saidi, S. L. Jacques and F. K. Tittel, "MIE AND RAYLEIGH MODELING OF VISIBLE-LIGHT SCATTERING IN NEONATAL SKIN," APPLIED OPTICS 34(31), 7410-7418 (1995)

8. A. M. Laughney, V. Krishnaswamy, P. B. Garcia-Allende, O. M. Conde, W. A. Wells, K. D. Paulsen and B. W. Pogue, "Automated classification of breast pathology using local measures of broadband reflectance," J Biomed Opt 15(6), 066019 (2010)

9. "Matlab Statistical Toolbox."

10. S. Wallis, "Binomial distributions, probability and Wilson's confidence interval," University College London (2009).

11. P. B. Garcia-Allende, V. Krishnaswamy, P. J. Hoopes, K. S. Samkoe, O. M. Conde and B. W. Pogue, "Automated identification of tumor microscopic morphology based on macroscopically measured scatter signatures," JOURNAL OF BIOMEDICAL OPTICS 14(3), 034034 (2009)

12. L. Gomez-Chova, Calpe, J., Camps-Valls, G., Martín, J.D., Soria, E., Vila, J., Alonso-Chorda, L., Moreno, J., "Feature selection of hyperspectral data through local correlation and SFFS for crop classification," IEEE International Geoscience Remote Sensing Symposium 1(555-557 (2003)